

The redshift and scale dependence of the cosmic shear signal from numerical simulations

Andrew J. Barber¹★

¹*Astronomy Centre, University of Sussex, Falmer, Brighton, BN1 9QJ.*

Accepted 2001 —. Received 2001 —; in original form 2001 —

ABSTRACT

The weak lensing shear signal has been measured numerically in N -body simulations at 14 different redshifts ($z_s = 0.1$ to 3.6) and on angular scales of $\theta = 2'$ to $32'$. In addition, the data have been validated by analytical computations for an identical cosmology, with density parameter $\Omega_m = 0.3$ and vacuum energy density parameter $\lambda_0 = 0.7$. This paper reports on the scale and redshift dependence of the shear variance, $\langle \gamma^2 \rangle$, which may be described by a simple formula of the form $\langle \gamma^2 \rangle(\theta, z_s) = a(\theta)z_s^{b(\theta)}$. The redshift dependence for source redshifts up to 1.6, is found to be close to z_s^2 , which is a stronger dependence than earlier analytical predictions ($\langle \gamma^2 \rangle \propto z_s^{1.52}$), although, at higher redshifts, the z_s dependence of the shear variance is clearly less steep. The strong redshift dependence further emphasises the need to know the precise redshift distribution for the galaxy sources in any given survey, so that they can be allocated to redshift bins accordingly, and the cosmic shear signal correctly interpreted. Equations are also given for the variance in the reduced shear, which is a more directly measurable quantity observationally.

Key words: Galaxies: clustering — Cosmology: gravitational lensing — Methods: numerical — Large-scale structure of Universe

1 INTRODUCTION

Studies of weak gravitational lensing in cosmology are a very powerful tool for attempts to understand the distribution of mass and the evolution of the large-scale structure in the universe. Recently, it has also become possible to constrain values for the cosmological parameters from weak lensing studies. Since the gravitational deflections of light arise from variations in the gravitational potential along the light path, the deflections result from the underlying distribution of mass which is usually considered to be in the form of dark matter. The lensing signal therefore contains information about the clustering of mass along the line-of-sight which may be different from the clustering inferred from galaxy surveys which trace the luminous matter only. In addition, by studying the way light from large numbers of sources at high redshifts is deflected, it is possible to obtain information about the way the clustering of mass evolves with time.

As a result of weak gravitational lensing, a source at high redshift will appear magnified (or de-magnified) as the beam converges (or diverges) due to matter (or an under-density) contained within it. The image also undergoes

shearing due to deflections from matter outside the beam, and causes a circular source, for example, to appear as an elliptical image. Sources at similar redshifts and contained within a small field-of-view will display similar magnification and shear characteristics because their light will have passed along similar density paths. For this reason there will be strong correlations in the changes to the ellipticities, particularly on small scales, and declining correlations on increasing angular scales.

The magnitude of this correlation depends strongly on the density parameter and the value of the cosmological constant for the universe, as these parameters reflect both the amount of mass and the rate of evolution of structure. A number of attempts have been made to estimate weak lensing statistics in different cosmological models, both analytically and numerically. See Bernardeau, Van Waerbeke & Mellier (1997), Jain & Seljak (1997) and Bacon, Refregier & Ellis (2000), for example, for analytical considerations, and Barber, Thomas & Couchman (1999), Jain, Seljak & White (2000), Barber et al. (2000), Hamana, Colombi & Mellier (2000), Van Waerbeke et al. (2001a) and Premadi et al. (2001), for example, for work done using various cosmological N -body simulations. These authors have attempted to predict values for various lensing statistics, many of which

★ Email: abarber@pact.cpes.susx.ac.uk

may be obtained directly or indirectly from observational data.

A number of observational results have now been reported for the so-called cosmic shear signal; see, for example, Bacon et al. (2000), Kaiser, Wilson & Luppino (2000), Maoli et al. (2001), Van Waerbeke et al. (2000a, b), Wittman et al. (2000), Mellier et al. (2001), Rhodes, Refregier & Groth (2001) and Van Waerbeke et al. (2001b). There is also a number of ongoing and planned observational programmes such as the Sloan Digital Sky Survey and surveys using the Visible and Infra-red Survey Telescope for Astronomy (VISTA). These and other telescope programmes will help to further constrain the cosmic shear values and the cosmological parameters. An excellent review of weak gravitational lensing and the measurement of the cosmic shear signal in particular is contained in the paper by Bartelmann & Schneider (2001).

The purpose of this paper is to predict important cosmic shear statistics using cosmological N -body simulations, which can be compared directly with observations. In particular, it reports the redshift and angular scale dependence for the shear variance and the reduced shear, computed numerically and supported by analytical computations. The detailed results are presented for background sources at 14 different redshifts and angular scales from $2'$ to $32'$. The finding that the shear variance has a strong redshift dependence draws attention to the need to have good redshift data in observational surveys before the cosmic shear signal can be correctly interpreted in terms of the underlying cosmology.

The numerical method uses the algorithm described in Couchman, Barber & Thomas (1999), which computes the three-dimensional shear in the simulations, and which has been applied to a simulation with density parameter $\Omega_m = 0.3$ and vacuum energy density parameter $\lambda_0 = 0.7$. (Cosmologies of this type will be referred to as LCDM cosmologies.) To obtain the required statistics on different angular scales, the computed shear values have been combined (using the appropriate angular diameter distance factors and accounting for multiple deflections) along lines of sight arranged radially from the observer's position at redshift $z = 0$. To support the numerical results, analytical computations have also been made for an identical cosmology, using the procedure of Van Waerbeke et al. (2001a).

A brief outline of this paper is as follows.

In **Section 2**, the equations and definitions required for weak lensing are presented, and analytical work to determine weak lensing statistics are described.

In **Section 3**, the shear algorithm and the N -body simulations are summarised together with details of the application of the code for the generation of the lensing statistics at the observer's location.

Section 4 presents the numerical results for the variances in the shear and the reduced shear for sources at different redshifts, and on different angular scales. Simple equations are presented which fit the data to describe these variances as functions of redshift and angular scale.

Section 5 is a discussion of the results.

2 WEAK LENSING THEORY

An explicit expression for each element of the three-dimensional shear at an arbitrary position, \mathbf{R} , arising from matter at positions \mathbf{R}' has been given by Barber et al. (2000):

$$\frac{\partial^2 \phi(\mathbf{R})}{\partial x_i \partial x_j} = -\frac{4\pi G}{3} a^2 \bar{\rho} \delta_{ij} + G \iiint \left[\frac{\rho(\mathbf{R}')}{|\mathbf{R} - \mathbf{R}'|^3} \delta_{ij} - \frac{3\rho(\mathbf{R}')(x_i - x'_i)(x_j - x'_j)}{|\mathbf{R} - \mathbf{R}'|^5} \right] d^3 R' \quad (1)$$

In this expression, ϕ is the peculiar gravitational potential, x_i and x_j are position coordinates, with the suffixes i and j representing the directions denoted by 1, 2 or 3, G is the universal gravitational constant, ρ and $\bar{\rho}$ are the density and mean density respectively, and a is the scale factor for the universe. The three-dimensional shear values computed by the shear algorithm can be identified with this expression.

To compute the required physical properties at $z = 0$ arising from the light of a distant source sheared by a *single* deflector, the quantities needed are the two-dimensional second derivatives of the effective lensing potential, which are denoted by ψ_{ij} , and which are calculated by integrating the three-dimensional shear along the coordinate direction x_3 , and including the appropriate angular diameter distance factors:

$$\psi_{ij} = \frac{D_d D_{ds}}{D_s} \cdot \frac{2}{c^2} \int \frac{\partial^2 \phi(x_3)}{\partial x_i \partial x_j} dx_3. \quad (2)$$

Here D_d , D_{ds} , and D_s are the angular diameter distances from the observer to the lens, the lens to the source, and the observer to the source, respectively, and c is the velocity of light in vacuo.

Where there are multiple deflections, these quantities, evaluated for the i th deflector (i is now used as the deflector index), form the elements of the shear tensor, $\mathcal{U}^{(i)}$, equivalent to the derivatives of the reduced deflection angle,

$$\mathcal{U}^{(i)} = \begin{pmatrix} \psi_{11}^{(i)} & \psi_{12}^{(i)} \\ \psi_{21}^{(i)} & \psi_{22}^{(i)} \end{pmatrix}. \quad (3)$$

By combining the $\mathcal{U}^{(i)}$ for all the deflectors, the final properties at $z = 0$ can be evaluated. To do this use is made of the multiple lens-plane theory, which has been described concisely by Schneider, Ehlers & Falco (1992). In this theory, Jacobian matrices, which describe how small changes in the position vector of an element of the source relate to small changes in the position vector of the corresponding element in the image, are constructed by recursion. The final Jacobian matrix, \mathcal{A} , at $z = 0$ resulting from N deflectors is given by

$$\mathcal{A} = \mathcal{I} - \sum_{i=1}^N \mathcal{U}^{(i)} \mathcal{A}^{(i)}, \quad (4)$$

where \mathcal{I} is the identity matrix, and in which the individual Jacobian matrices are

$$\mathcal{A}^{(j)} = \mathcal{I} - \sum_{i=1}^{j-1} \beta_{ij} \mathcal{U}^{(i)} \mathcal{A}^{(i)} \quad (5)$$

for the j th lens, and

$$\mathcal{A}^{(1)} = \mathcal{I} \quad (6)$$

for the first lens. In equation 5,

$$\beta_{ij} \equiv \frac{D_s}{D_{is}} \frac{D_{ij}}{D_j}, \quad (7)$$

where D_s and D_j are the angular diameter distances to the source and the j th lens respectively, and D_{is} and D_{ij} are the angular diameter distances from the i th lens to the source and the i th lens to the j th lens respectively. The final Jacobian can be written in the form

$$\mathcal{A} = \begin{pmatrix} 1 - \psi_{11} & -\psi_{12} \\ -\psi_{21} & 1 - \psi_{22} \end{pmatrix}, \quad (8)$$

from which the components of the overall two-dimensional shear, γ , for weak lensing are

$$\gamma_1 = \frac{1}{2}(\psi_{11} - \psi_{22}) \quad (9)$$

and

$$\gamma_2 = \psi_{21} = \psi_{12}. \quad (10)$$

(In a weak shear field smoothed by the variable particle softening and where the gravitational potential and its derivatives are well-behaved continuous functions, $\psi_{21} \simeq \psi_{12}$.) The two-dimensional shear is

$$\gamma = \gamma_1 + i\gamma_2 \quad (11)$$

($i \equiv \sqrt{-1}$), and the orientation of the major axis of the resulting elliptical image is

$$\phi = \frac{1}{2}\tan\left(\frac{\gamma_2}{\gamma_1}\right). \quad (12)$$

The effective convergence is

$$\kappa = \frac{1}{2}(\psi_{11} + \psi_{22}), \quad (13)$$

and the final magnification is

$$\mu = (\det \mathcal{A})^{-1} = \frac{1}{(1 - \kappa)^2 - \gamma^2}. \quad (14)$$

Since the shear causes the axes to be stretched by factors of

$$a = (1 - \kappa - |\gamma|)^{-1} \quad (\text{major axis}) \quad (15)$$

and

$$b = (1 - \kappa + |\gamma|)^{-1} \quad (\text{minor axis}), \quad (16)$$

the imposed ellipticity can easily be calculated from the elements of the Jacobian matrix. Observationally, the ellipticity of an image is frequently defined in terms of the tensor of second brightness moments,

$$Q_{ij} = \frac{\int d\theta q_I[I(\theta)](\theta_i - \bar{\theta}_i)(\theta_j - \bar{\theta}_j)}{\int d\theta q_I}[I(\theta)], \quad (17)$$

where $I(\theta)$ is the surface brightness of the galaxy image at angular position θ , $\bar{\theta}$ is the angular position of the centre of light, and $q_I[I(\theta)]$ is a weighting function in terms of the surface brightness. (See Blandford et al., 1991, for example.) Then one definition is the complex ellipticity

$$\epsilon = \frac{Q_{11} - Q_{22} + 2iQ_{12}}{Q_{11} + Q_{22} + 2(Q_{11}Q_{22} - Q_{12}^2)^{\frac{1}{2}}}. \quad (18)$$

For elliptical isophotes, this definition is equivalent to

$$\epsilon = \frac{1 - r}{1 + r} e^{2i\phi}, \quad (19)$$

where $r \equiv b/a$.

The “reduced shear,” g , evaluated for position θ in the image, is defined by

$$g(\theta) \equiv \frac{\gamma(\theta)}{1 - \kappa(\theta)}, \quad (20)$$

so that the transformation between the source and image ellipticities may be given by

$$\epsilon^{(s)} = \frac{\epsilon - g}{1 - g^* \epsilon} \quad (21)$$

for $|g| \leq 1$ (where the asterisk refers to the complex conjugate).

Then, in the case of weak lensing, for which κ and $|\gamma| \ll 1$, $|g| \ll 1$, so that, for low intrinsic source ellipticities, $\epsilon \simeq \epsilon^{(s)} + g$.

However, the intrinsic ellipticities of observed galaxies are generally unknown, so that the determination of the shear signal from individual images is impossible. For this reason, it is necessary to consider ensembles of galaxy images together, and to assume that the galaxies of each ensemble have random intrinsic ellipticities, so that the ensemble has zero net ellipticity. Whilst this is strictly not true, in high-redshift surveys in which the galaxies within each narrow cone may be widely separated, it serves as a good working approximation. A number of studies have been made into intrinsic correlations of galaxy shapes; Heavens, Refregier & Heymans (2000), for example, have shown that the intrinsic correlation function for elliptical galaxies at $z = 1$ in an LCDM cosmology is only of order 10^{-4} on angular scales of $0.1'$ to $10'$, and is approximately an order of magnitude lower than the correlations expected from weak lensing. However, the intrinsic correlations are expected to exceed those arising from weak shear in shallow surveys, as found, for example by Brown et al. (2000), for sources with a median redshift of only 0.1.

If then the ensemble of sources has zero net ellipticity, $\langle \epsilon^{(s)} \rangle = 0$ and

$$\langle \epsilon \rangle = \frac{\sum_i u_i \epsilon_i}{\sum_i u_i} \simeq g, \quad (22)$$

where the u_i are weight factors. Consequently then, in the case of weak lensing only,

$$\gamma \simeq g \simeq \langle \epsilon \rangle, \quad (23)$$

and the variances in both the shear and the reduced shear for a given angular scale are expected to be similar.

The importance of the convergence for understanding the evolution of structure lies in its close association with the density contrast, $\delta(\mathbf{x})$, at position \mathbf{x} , which is defined by

$$\delta(\mathbf{x}) \equiv \frac{\rho(\mathbf{x}) - \bar{\rho}}{\bar{\rho}}. \quad (24)$$

By extension of the above equations for ψ_{ij} (equation 2) and κ (equation 13), twice the value of the effective convergence in the direction θ for a source at distance x_s is

$$2\kappa(\theta, x_s) = \int_0^{x_s} \frac{D(x_3)D(x_s - x_3)}{D(x_s)} (\nabla^2 - \nabla_{x_s}^2) \phi(\theta, x_3) dx_3$$

$$\simeq \int_0^{x_s} \frac{D(x_3)D(x_s - x_3)}{D(x_s)} \nabla^2 \phi(\theta, x_3) dx_3, \quad (25)$$

in which

$$\nabla^2 \phi(\theta, x_3) = \frac{3H_0^2}{2} \Omega_m \frac{\delta(\theta, x_3)}{a(x_3)}, \quad (26)$$

where H_0 is the Hubble parameter. Consequently, the effective convergence represents a projection of the density contrast, and is proportional to the density parameter, Ω_m :

$$2\kappa(\theta, x_s) \simeq \frac{3H_0^2}{2} \Omega_m \int_0^{x_s} \frac{D(x_3)D(x_s - x_3)}{D(x_s)} \frac{\delta(\theta, x_3)}{a(x_3)} dx_3. \quad (27)$$

It is also important to note how the two-point statistical properties of the shear and convergence are related. From the definitions of the individual shear tensors, \mathcal{U}^i (equation 3), the components γ_1 and γ_2 of the shear (equations 9 and 10), and the effective convergence, κ (equation 13), the following expressions apply in Fourier space:

$$\tilde{\gamma}_1(\mathbf{l}) = \frac{l_1^2 - l_2^2}{l^2} \tilde{\kappa}(\mathbf{l}), \quad (28)$$

and

$$\tilde{\gamma}_2(\mathbf{l}) = \frac{2l_1 l_2}{l^2} \tilde{\kappa}(\mathbf{l}), \quad (29)$$

where l_1 and l_2 are the components of the wavevector \mathbf{l} , so that

$$\tilde{\gamma}_1^2(\mathbf{l}) + \tilde{\gamma}_2^2(\mathbf{l}) = \tilde{\kappa}^2(\mathbf{l}). \quad (30)$$

Then it is clear that the power spectra for the shear, $P_\gamma(l)$, and the convergence, $P_\kappa(l)$, are the same in the case of weak lensing.

To obtain values for the shear (or convergence) variances analytically, the convergence power spectrum is integrated over all wavenumbers, using a filter function appropriate for the required angular scale, θ . Since the convergence is obtained from a projection of the density contrast (equation 27) from the source redshift to the observer, the shear variance calculation requires a complete spatial and temporal description of the matter power spectrum, $P_\delta(k, x)$. This is a function of the real-space wavenumber, k ($= l/(D(x)\theta)$, where $D(x)$ is the angular diameter distance for a radial distance x from the observer. Kaiser (1998) has determined general expressions for the angular power spectra of weak lensing distortions for different cosmological models, and has estimated the growth of this power with source redshift. As expected, the redshift dependence is much stronger in low density cosmologies and especially so in cosmologies dominated by a cosmological constant.

Jain & Seljak (1997) give an expression equivalent to the following for the shear variances derived analytically from the matter power spectrum.

$$\langle \gamma^2 \rangle(\vartheta) = \frac{1}{4} \times 36\pi^2 \Omega_m^2 \int_0^\infty k dk \times \int_0^{x_s} a^{-2}(x) P_\delta(k, x) G^2(x) W_2^2[kD(x)\vartheta] dx, \quad (31)$$

where x_s is the radial distance to the source,

$$G(x) = \frac{D(x)D(x_s - x)}{D(x_s)} \quad (32)$$

and

$$W_2[kD(x)\vartheta] = 2J_1[kD(x)\vartheta]/[kD(x)\vartheta], \quad (33)$$

where J_1 is the first Bessel function of the first order. The scale ϑ is the angular radius of a circular window, so that the formula has to be transformed to express the shear variance on scales, θ , represented by square pixels.

A complete description of the power spectrum on all scales (including the linear, quasi-linear and non-linear regimes) is necessary for the analytical approach, together with a detailed description of its evolution. In particular, non-linear effects on scales of order $1'$ may increase the amplitude of the convergence power spectrum by an order of magnitude. In addition, density fluctuations on scales smaller than about $10'$ contribute most strongly to the weak lensing signal, precisely where the non-linear evolution of the power spectrum is most in evidence. In the non-linear regime, the fitting formulae of Peacock & Dodds (1996), which extends the earlier work of Hamilton et al., (1991) for the evolution of the matter correlation function, may be used to map the non-linear wavenumbers onto equivalent linear wavenumbers, and thus to evaluate the shear variance values. These fitting formulae include the stable-clustering hypothesis which assumes an invariant mean particle separation on sufficiently small scales. Analytical programs based on this prescription are accurate to $\sim 15\%$, depending on the cosmological model.

For (circular) angular scales of $\vartheta = 2'$ and $15'$, Jain & Seljak (1997) summarised their findings in approximate power-law expressions, which are equivalent to

$$\langle \gamma^2 \rangle[\vartheta = 2'(15')] \propto \vartheta^{-0.84} z_s^{1.52} \sigma_8^{2.58(2.00)} \Omega_m^{1.20(1.36)} \quad (34)$$

for LCDM cosmologies. The different indices for σ_8 and Ω_m on the different scales enable the degeneracy between these parameters to be lifted when measurements are made in both regimes. The power of z_s quoted is an intermediate value for the two angular scales.

On the scales $1' < \vartheta < 30'$, the angular scale dependency was similar, and the powers of z_s were close; the index of z_s decreased from 1.54 at $\vartheta = 2'$ to 1.48 at $\vartheta = 15'$. As a result, Jain & Seljak (1997) found that, for LCDM cosmologies,

$$\langle \gamma^2 \rangle(\theta) \propto \theta^{-0.84} z_s^{1.52} \quad (1' < \theta < 30') \quad (35)$$

approximately. (ϑ and θ are interchangeable in this context.)

The numerically determined shear variance results quoted in this paper, and derived from the real-space values of the shear computed numerically, will be compared with this approximate expression. In addition, as a check of the validity of the numerical results, analytical values for the shear variance have also been computed directly for the precise cosmology used in the numerical simulations. To achieve this the analytical program described in Van Waerbeke et al. (2001a) has been used, which is a quite general program for determining the weak lensing statistics in different cosmologies. For the non-linear evolution of the power spectrum (and the determination of variances), the fitting formulae of Peacock & Dodds (1996) are used. For higher-order statistics, such as the weak lensing skewness (not computed in this work), the code also computes the evolution of the bispectrum at all scales, based on fitting formulae derived by Scoccimarro & Couchman (2001) in numerical simulations.

3 NUMERICAL PROCEDURE

Couchman et al. (1999) describe in detail the algorithm for the computation of the elements of the matrix of second derivatives of the gravitational potential in cosmological N -body simulations. It computes all of the six independent component values of the three-dimensional shear at each of the selected evaluation positions. The rms errors in the computed shear component values are typically $\sim 0.3\%$.

The algorithm uses a variable particle softening which distributes the mass of each particle throughout a radius which depends on its specific environment. The actual values of the softening parameters are precisely as described in Barber et al. (2000), with the minimum value set to $0.1h^{-1}\text{Mpc}$ throughout, where h is the Hubble parameter expressed in units of $100\text{km s}^{-1}\text{Mpc}^{-1}$.

In the computation of the shear, the code uses the peculiar gravitational potential, ϕ , through the subtraction of a term depending upon the mean density. This ensures that only light ray deflections arising from departures from homogeneity apply, and is equivalent to requiring that the net total mass in the system be set to zero. The algorithm automatically includes the contributions of the periodic images of the fundamental volume in computing the three-dimensional shear at any location, thereby essentially creating a realisation extending to infinity.

Since the algorithm works within three-dimensional simulation volumes, rather than on planar projections of the particle distributions, angular diameter distances to every evaluation position can be applied. In this work it has been assumed that the angular diameter distance varies linearly through the depth of each simulation volume.

The code has been applied to the cosmological N -body simulations of the Hydra Consortium[†] produced using the ‘Hydra’ N -body hydrodynamics code (Couchman, Thomas & Pearce, 1995). Simulations of the LCDM Dark Matter only cosmology were used with $\Omega_m = 0.3$, $\lambda_0 = 0.7$, power spectrum shape parameter $\Gamma = 0.25$ and normalisation, σ_8 , on scales of $8h^{-1}\text{Mpc}$ of 1.22. The number of particles, each of mass $1.29 \times 10^{11}h^{-1}$ solar masses, was 86^3 and the simulation boxes had comoving side dimensions of $100h^{-1}\text{Mpc}$. The simulation output times were chosen so that consecutive simulation boxes could be abutted. A total of 48 boxes to a redshift of 3.57 in the LCDM cosmology were used. To avoid obvious structure correlations between adjacent boxes, each was arbitrarily translated, rotated (by multiples of 90°) and reflected about each coordinate axis, and in addition, each complete run was performed 20 times, so that averages of the final statistics were determined to represent the required results.

To follow the behaviour of light rays from distant sources through the simulation boxes, and obtain distributions of the properties at $z = 0$, a set of light paths was constructed emanating from the centre of the front face of the $z = 0$ box and ending in a regular square array of locations at the plane of the chosen source redshift.

A total of 14 source redshifts were selected to give good statistical coverage of the redshifts of interest. These were redshifts of $z_s = 0.10, 0.21, 0.29, 0.41, 0.49, 0.58, 0.72, 0.82$,

0.88, 0.99, 1.53, 1.97, 3.07 and 3.57. They corresponded to the simulation box redshifts and were chosen to be close to redshifts of 0.1, 0.2, 0.3, 0.4, 0.5, 0.6, 0.7, 0.8, 0.9, 1.0, 1.5, 2.0, 3.0 and 3.5. In this paper the source redshifts will be referred to loosely as the latter approximate values, although in the determination of redshift dependences, etc., the actual redshift values were used.

Using a total of 317×317 lines of sight, the angular size of the minimum particle softening is comparable to or less than the angular separation of the adjacent lines of sight ($0'.49$) for all redshifts greater than 0.14. Consequently, to account for the larger angular size of the minimum softening at low redshifts, and also for the allowed range of particle softening scales above the minimum value, a resolution limit of $2'$ has been adopted for the data analyses. In addition, the angular size of the gravitational force softening used in the generation of the simulation boxes is below the line-of-sight separation for all redshifts greater than 0.05. For a source at redshift 1 in the LCDM cosmology, maximal gravitational lensing occurs for a lens at redshift 0.36, and the angular separation of adjacent lines of sight is approximately the same value as the angular size of the minimum particle softening at that redshift ($0'.47$).

The total field-of-view for the set of lines of sight was $2.6^\circ \times 2.6^\circ$, and this completely fills the near face of the simulation box at redshift 1.0.

To establish the locations for the evaluation of the shear on each of the lines of sight, first a regularly spaced (coarse) set of 50 locations was laid down on each line in each simulation box. Then additional locations were computed at positions where the gravitational potential was changing most rapidly, so that the potential field could be well-sampled. To establish these locations, the particles were assigned to volumes determined by a 10×10 grid within each box. From each of the coarse line of sight locations, the separations to the particles within the local grid volume and the nearest neighbouring grid volumes was determined. If a separation was less than the line-of-sight separation, a new evaluation location was established on the line-of-sight, with coordinates corresponding to the particle’s position in the x_3 direction (radially from the observer). All the evaluation locations (coarse and new) along each line in each box were then sorted, labelled and counted so that the programme to integrate the values along the lines of sight would operate in the correct order for the correct number of locations.

Following the shear computations at all of the locations on all the lines of sight in all the simulation volumes, the second derivatives of the two-dimensional effective lensing potentials were obtained from the three-dimensional shear values by integration, in accordance with equation 2. The integration was made in step-sizes determined by the separation of adjacent evaluation locations on each of the lines of sight, and so was different for every pair of points. The integration algorithm was set to run from each of the chosen source redshift planes, along each of the lines of sight to $z = 0$, and values for the elements of the shear matrix, and thus the Jacobian matrix, at the observer were obtained for each of the lines of sight. From these data, all the required weak lensing statistics were obtained for each line of sight and for each source redshift.

The full procedure, from the computation of the three-dimensional shear values at all the evaluation locations to

[†] (<http://hydra.mcmaster.ca/hydra/index.html>)

finally obtaining the Jacobian matrices at $z = 0$, involved precisely the same approximations as described fully in Barber et al. (2000). In addition, it should be noted that, because the lines of sight project radially from the observer at $z = 0$, some lines of sight pass outside the confines of the simulation volume beyond a redshift of 1. In these cases, the periodicity of the boxes has been used to reposition the lines of sight at equivalent locations within the volumes. The area of the far face of the most distant simulation box (at redshift 3.6) is $1.3^\circ \times 1.3^\circ$. Consequently, the procedure is not expected to introduce significant effects on the computed variances on the scales of interest here, which are up to a maximum of $32'$.

4 RESULTS

The individual real-space values for the shear, γ , and the reduced shear, g , were computed from the final Jacobian matrices obtained in each run for each line-of-sight and for each source redshift. These data sets were then separately convolved with a top-hat smoothing function of the required scale-size, and the statistical variance values obtained on those specified scales. The scale-sizes chosen for the top-hat smoothing were $2'$ (consistent with the resolution limit of the numerical procedure), $4'$, $8'$, $16'$ and $32'$. The computed values from each of the N runs were then averaged, and the errors on the means of $1\sigma/\sqrt{N}$ determined.

Figure 1 shows the shear variances computed in this way (without the error bars for clarity) for all the source redshifts, with the exception of $z_s = 0.1$, which is too low to be seen clearly. The figure clearly emphasises the redshift dependence of the results and suggests that a good knowledge of the redshift distribution of the sources observed in surveys is essential to interpreting the shear signal correctly. The relative closeness of adjacent curves separated by intervals of only 0.1 in redshift also suggests that the shear signal from sources with a *small* spread in redshift *may* be adequately described by the shear signal expected from sources at their median redshift.

However, it is not clear that the shear resulting from sources with a significant redshift distribution will be representative of the shear from sources at their median redshift.

A number of recent measurements of cosmic shear have been made, as mentioned in the Introduction. Following these measurements, Kaiser et al. (2000) and Bartelmann & Schneider (2001) have plotted them on a single diagram and compared the results with the predicted values for the shear variances as suggested by Jain & Seljak (1997), whose work is described above. As can be seen from the diagrams in these references, the cosmic shear signal resulting from all the observed measurements (from different telescopes, filters and cameras, and different fields of view and data analysis techniques), appears to lie very close to the formerly predicted values for sources at a redshift of 1.

The numerical values computed here for source redshifts of 0.4, 0.6, 0.8, 1.0 and 1.5 are now plotted in figure 2, together with the analytical values determined using Van Waerbeke et al.s (2001a) code, described above; also shown are Jain & Seljak's (1997) predicted values (transformed to square pixel areas) for source redshifts of 1, using their approximate expression for general LCDM cosmologies. The

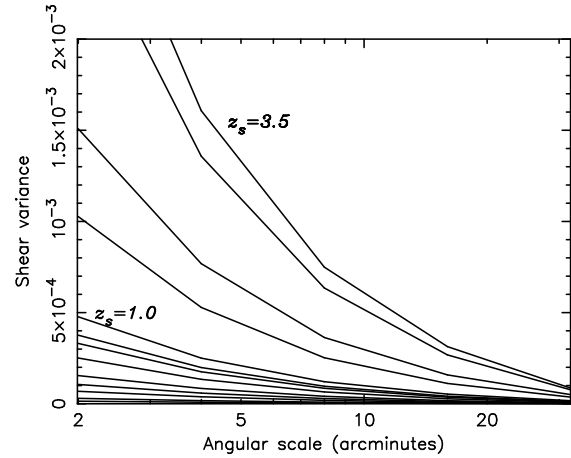


Figure 1. $\langle \gamma^2(\theta) \rangle$ for source redshifts 0.2 (lowest curve), 0.3, 0.4, 0.5, 0.6, 0.7, 0.8, 0.9, 1.0, 1.5, 2.0, 3.0 and 3.5 (uppermost curve).

advantage of Van Waerbeke et al's (2001a) prescription is that the precise cosmological parameters and source redshifts used in the numerical work have been used.

The numerically computed values for $z_s = 1$ are remarkably close to the values predicted analytically by both Jain & Seljak (1997) and Van Waerbeke et al.s (2001a) prescription. In particular, the analytical results computed here give strong support to the numerical results, and the agreement is particularly good at low redshift and at intermediate angular scales. The largest discrepancies occur only for sources at high redshift (beyond about 1.5) and at angular scales comparable with and below the resolution limit of the numerical data, and where breakdown of both the numerical and analytical procedures may also be expected. The values from Jain & Seljak's (1997) approximate general expression differ somewhat from both the numerical and analytical results reported here for source redshifts other than 1, so that it appears qualitatively that the results here would show a different redshift dependence than the former analytical predictions.

The redshift dependence of the shear variance on the chosen angular scales is now plotted in figure 3.

Since the redshift relationship for the shear variance and its scale dependence are of fundamental importance to observational measurements of the cosmic shear signal, the numerical results from figures 1, 2 and 3 have been fitted mathematically. It is assumed that the shear variance can be expressed in the simple form

$$\langle \gamma^2 \rangle(\theta, z_s) = a(\theta)z_s^{b(\theta)}, \quad (36)$$

and indeed, for the redshift range $z_s \leq 1.6$, this form describes the shear variances well.

Over the range of angular scales $2'$ to $32'$, the coefficient $a(\theta)$ can be expressed as

$$a(\theta) = (1.05 \pm 0.05) \times 10^{-3} \theta^{-1.12 \pm 0.03}, \quad (37)$$

for θ in arcminutes. At the low end of the range of scales, the index $b(\theta)$ falls very slightly as θ increases, and then remains almost constant to beyond $32'$. Hence, for the entire range

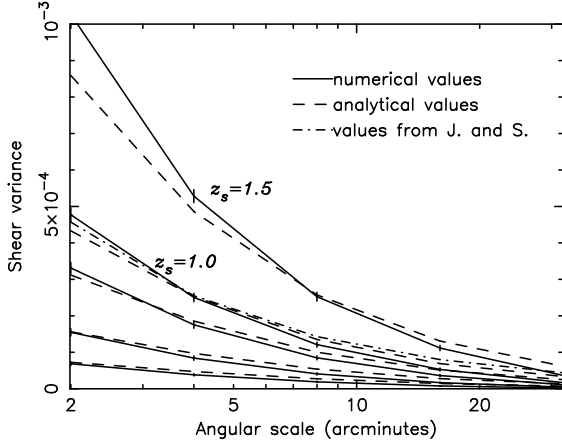


Figure 2. The numerical shear variances and analytical values computed here, based on an identical cosmology and the same source redshifts. Source redshifts of 0.4 (lowest pair of curves), 0.6, 0.8, 1.0 and 1.5 (uppermost pair of curves) are plotted, respectively. For comparison, the analytical predictions of Jain & Seljak (1997) for sources at a redshift of 1 are also plotted, based on their approximate general expression for LCDM cosmologies.

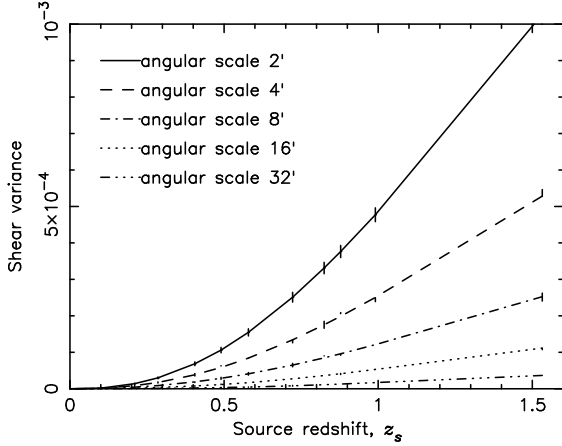


Figure 3. $\langle \gamma^2(\theta, z_s) \rangle$ as a function of source redshift for angular scales of 2', 4', 8', 16' and 32'.

of scales 2' to 32', $b(\theta)$ can be described well by the constant value

$$b(\theta) = 2.07 \pm 0.04. \quad (38)$$

The relationships amongst $\langle \gamma^2 \rangle$, θ and z_s may be seen more clearly in figure 4 for the numerical data, which has logarithmic axes. At low redshifts the slopes of the curves have a very small θ dependence, and, for redshifts greater than about 1, the curves become clearly less steep, indicating that the redshift dependence falls well below 2 at high source redshifts.

In Section 2, it was shown that, in the case of weak lensing, both the shear, γ , and the reduced shear, g , will be approximately equal, so that the variances in both these

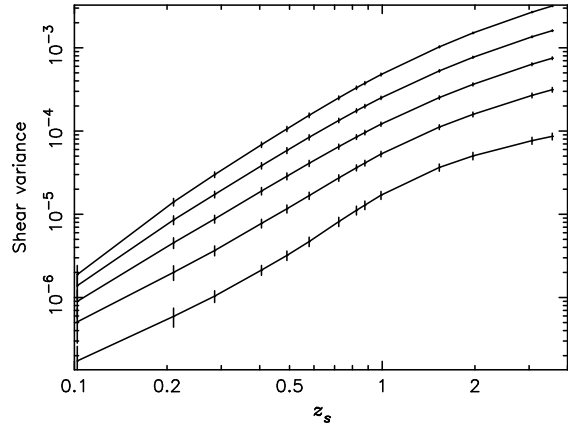


Figure 4. $\langle \gamma^2(\theta) \rangle$ vs. z_s on logarithmic axes, to show the gradually declining slopes at high redshift for the measured shear variances. The curves are for angular scales of 2' (uppermost curve), 4', 8', 16' and 32' (lowest curve).

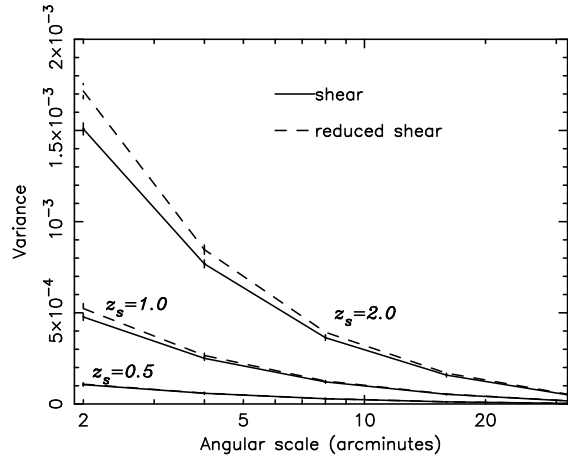


Figure 5. The variances in the reduced shear and the shear for comparison, for source redshifts of 0.5, 1.0 and 2.0.

quantities will also be similar. Indeed, this approximation is used observationally to estimate the values of the shear from the observed ellipticities. However, the equality holds only in the weak lensing limit. The numerical method used here for computing the weak lensing statistics enables a direct comparison to be made between the variances in γ and g .

Figure 5 compares $\langle g^2 \rangle(\theta)$ with $\langle \gamma^2 \rangle(\theta)$ for redshifts of 0.5, 1 and 2. For low source redshifts, the curves are almost identical (except for the smallest of angular scales). This is as expected, because this is the regime of the weak lensing limit. However, departures between the two quantities become increasingly obvious as the source redshift is increased.

The redshift dependence for $\langle g^2 \rangle$ on the different angular scales is plotted in figure 6.

The functional form of $\langle g^2 \rangle(\theta, z_s)$ can be written in a similar way to that for $\langle \gamma^2 \rangle(\theta, z_s)$. By analogy with equa-

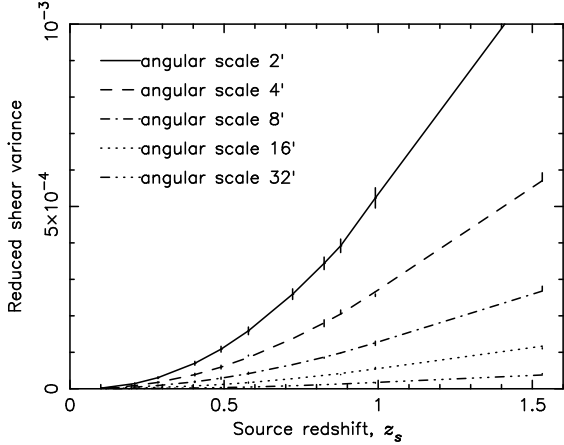


Figure 6. $\langle g^2(\theta, z_s) \rangle$ as a function of redshift for the angular scales of $2'$, $4'$, $8'$, $16'$ and $32'$.

tion 36, the variance in the reduced shear can be written as

$$\langle g^2 \rangle(\theta, z_s) = c(\theta) z_s^{d(\theta)} \quad (39)$$

in the range $z_s \leq 1.6$, for $2' \leq \theta \leq 32'$.

The coefficient $c(\theta)$ can be expressed as

$$c(\theta) = (1.2 \pm 0.1) \times 10^{-3} \theta^{-1.21 \pm 0.03}. \quad (40)$$

As for $b(\theta)$ in the expression for the shear variance, $d(\theta)$ here falls very slightly as θ increases at small angular scales, but then remains almost constant throughout the range of angular scales. Explicitly, for $2' \leq \theta \leq 32'$, $d(\theta)$ can be expressed as the constant value

$$d(\theta) = 2.01 \pm 0.04. \quad (41)$$

The variance in the reduced shear for the entire redshift range is plotted with logarithmic axes in figure 7 to indicate both the θ and z_s dependencies of the results.

As found for the shear variance, figure 7 for the reduced shear, shows how the slopes of the curves at the low redshift end have a slight θ dependence. However, unlike the shear, at high redshifts the slopes become more noisy and generally steeper, even though the slopes do decline very gently throughout the redshift range up to about 2. This is most likely a result of the sensitivity to the convergence, apparent from equation 20, which becomes important either on small angular scales or at high redshifts, where the lensing effects are strongest.

5 DISCUSSION AND CONCLUSIONS

The main results established in this paper are the dependences of the shear variance and the variance in the reduced shear on source redshift and angular scale. The numerical data obtained has been validated by analytical computations using Van Waerbeke et al.'s (2001a) program applied to an identical cosmology and the same source redshifts.

For the shear variance, for source redshifts up to 1.6, one can write, without the error bars for clarity,

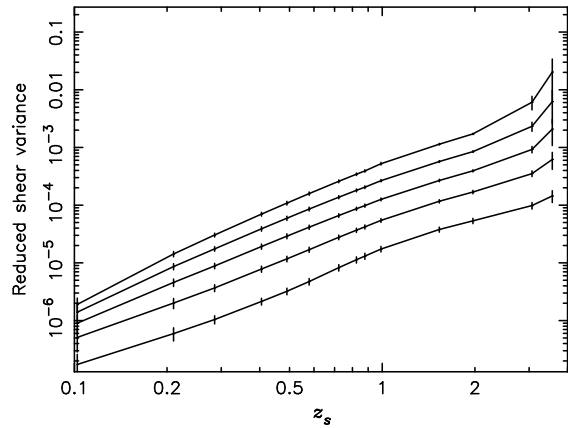


Figure 7. $\log(\langle g^2(\theta) \rangle)$ vs. $\log(z_s)$, to show the gradually declining slopes throughout most of the redshift range for the reduced shear variances on angular scales of $2'$ (uppermost curve), $4'$, $8'$, $16'$ and $32'$ (lowest curve).

$$\langle \gamma^2 \rangle(\theta, z_s) = 1.05 \times 10^{-3} \theta^{-1.12} z_s^{2.07} \quad (42)$$

for $2' \leq \theta \leq 32'$. I.e., the redshift dependence is close to z_s^2 , and stronger than the previous analytical predictions of Jain & Seljak (1997) who found a dependence close to $z_s^{1.52}$. Whilst the above equation fits the numerical data well within the range specified, the redshift dependence clearly begins to decline for sources beyond a redshift of 1, so that the index of z_s falls substantially below 2 at high redshift.

For the variance in the reduced shear, again it has been found that the redshift dependence is close to z_s^2 , and for $z_s \leq 1.6$ it can be described by

$$\langle g^2 \rangle(\theta, z_s) = 1.2 \times 10^{-3} \theta^{-1.21} z_s^{2.01} \quad (43)$$

for $2' \leq \theta \leq 32'$, again without the error bars for clarity. At higher redshifts, although there is an underlying tendency for the curves to become less steep, the reduced shear is noisy and sensitive to values of the convergence, so that the curves steepen again at the high redshift end.

It was mentioned in the Results section that Kaiser et al. (2000) and Bartelmann & Schneider (2001) have plotted recent observational determinations of the shear variances on a single diagram and compared the results with the predicted analytical values of Jain & Seljak (1997). These plots show the observational results to lie close to the predicted curve for sources at a redshift of 1. It should be noted at this point that the values determined numerically here, and also analytically using Van Waerbeke et al.'s (2001a) program, concur well with the analytical values plotted for source redshifts of 1. However, the observational results plotted have galaxies with distributions in redshift; for example, Bacon et al. (2000) quote a median redshift of $z_s = 0.8 \pm 0.2$ for their sample, Van Waerbeke et al. (2000a) refer to a peak redshift of 0.9 for their galaxies, Kaiser et al. (2000) has an "effective" redshift of 1.0, and the survey of Maoli et al. (2001) has a broad redshift distribution which peaks at a redshift of 0.8.

Whilst Jain et al. (2000) claim that a distribution of sources with a mean redshift of 1 gives rise to an amplitude

for the shear variance only 10% different from the case where all the galaxies are assumed to lie at $z_s = 1$, the contention here is that it is necessary to have a clear understanding of how the shear signal relates to the redshift of the sources, and how a distribution of source redshifts may further influence the conclusions. As an example, there are differences of $\sim 10\% - 20\%$ between the shear variance values for sources separated by a redshift interval of only 0.1 on angular scales of $2'$. Attempts to constrain the cosmology precisely will founder if the redshift dependence reported here is not taken into account. According to equation 34 an uncertainty of about 0.025 in the density parameter also results if there is a 10% uncertainty in the shear variance. In addition, there are clear differences between the variances in the shear and the more directly measured reduced shear, particularly at high redshift and on small angular scales where the weak-lensing regime may not be applicable. These factors point clearly to the need for studies into the strength of the cosmic shear signal for sources distributed in redshift, and will be investigated in a future paper.

The faster redshift dependence reported here ($\sim z_z^{2.07}$ compared with $\sim z_z^{1.52}$ previously predicted) is not easily explained, as there are assumptions in both approaches. In the numerical method one could point to the discontinuities in structure as one passes from box to box, although the effect of this is reduced statistically by employing a large number of runs (20 in this work). The particle softening and resolution limitations might also be a factor in the simulations. In the analytical approach, the main difficulty arises in trying to describe accurately the evolution of the power spectrum in the non-linear regime. Here mapping techniques using fitting formulæ, accurate to $\sim 15\%$, are used to relate the linear and non-linear spectra, and assumptions such as the stable-clustering hypothesis are used. Also, Jain & Seljak's (1997) published predictions are the result of summarising data from different cosmological models, and then fitting the data to approximate formulae to express the power-law dependencies of the statistics. Improvements have been made more recently however in analytical procedures, for example, Seljak (2000) and Peacock & Smith (2000) have developed a model for the non-linear evolution of the power spectrum based on the random distribution of dark matter haloes, modulated by the large-scale matter distribution.

The main advantage of the numerical method is that the shear values and variances are determined directly from the real-space data, rather than from integration of a power spectrum which is less well understood on the scales of interest. It is also expected that numerical results may be used in the future to test the validity of developments in analytical procedures, which will be increasingly needed in view of the expected accuracies in the next generation of cosmic shear measurements. For the interpretation of these observations, fast analytical procedures will be more practical, since it will be unrealistic to generate large numbers of numerical simulations to cover a realistic parameter space.

A key influence on the redshift dependence of the shear variance lies in the functional form of $\mathcal{G}(x)$, the angular diameter distance function. $\mathcal{G}(x)$ occurs in equation 31 where it multiplies the matter power spectrum to produce the effective convergence power spectrum. In the numerical method here it also plays a crucial role in establishing the elements of the final Jacobian matrices, from which the convergence and

shear values are obtained. In the numerical work here, the ‘‘filled beam’’ values for $\mathcal{G}(x)$ have been used as it is assumed that the light is always passing through a region of smoothed density. (See Barber et al., 2000, for a full discussion of angular diameter distances in inhomogeneous universes.) The form of $\mathcal{G}(x)$ at high redshifts may also help to explain the reducing index of z_s , because the redshift value at the peak of the $\mathcal{G}(x)$ curve rises less quickly as the source redshift is increased.

In this paper, no attempt has been made to simulate the signal which might arise from typical noisy data. The intrinsic ellipticities of the background galaxies is a source of random noise, and in addition, measurement errors of very faint galaxies introduce errors in the ellipticity estimates.

The intrinsic ellipticity correlations of galaxies in close proximity to each other produce a real signal which has to be disentangled from the cosmic shear correlations from the large-scale structure along the line-of-sight. Heavens et al. (2000) have attempted to determine the intrinsic correlations by modelling the shapes and angular momentum vectors of galaxies in a way which reflects the shape and angular momenta of their dark matter halos in N -body simulations. They find that the intrinsic ellipticity correlation function for elliptical galaxies is an order of magnitude below the expected weak lensing signal on scales of $0.1'$ to $10'$ for sources at $z_s = 1$ in a Λ CDM cosmology. Brown et al. (2000) have analysed real data from the SuperCOSMOS Sky Survey for galaxies with a low median redshift of $z_s = 0.1$. They find that the ellipticity variance is approximately two orders of magnitude higher than the expected weak lensing signal throughout the range $1'$ to $100'$. As the source redshifts are low, they claim that their result represents the real intrinsic correlations since the weak lensing signal would be expected to be small.

Taking the above two reports into account, there will be some intermediate redshift at which the weak lensing signal overtakes the intrinsic one. Consequently, whilst the result reported here presents the pure redshift dependency of the weak lensing signal, it is clearly advantageous to study good data at high redshift in order to measure the uncontaminated cosmic signal.

This represents a further argument in favour of having good redshift information in a galaxy survey designed to measure cosmic shear. It is anticipated that forthcoming deep weak lensing surveys, such as that proposed for the VISTA telescope, will also provide detailed photometric redshift information to enable the surveyed galaxies to be binned in redshift intervals. In this way it is anticipated that the real cosmic shear signal may be interpreted more correctly.

ACKNOWLEDGEMENTS

This work has been supported by PPARC and carried out with facilities provided by the University of Sussex. The original code for the three-dimensional shear computations was written by Hugh Couchman of McMaster University. There were many useful discussions with Andy Taylor, Antonio da Silva, Peter Thomas, Rachel Webster and Andrew Melatos. The program to perform the analytical computations was kindly provided by Ludo Van Waerbeke.

REFERENCES

Bacon D. J., Refregier A. R., Ellis R. S., 2000, MNRAS, 318, 625
 Barber A. J., Thomas P. A., Couchman H. M. P., 1999, MNRAS, 310, 453
 Barber A. J., Thomas P. A., Couchman H. M. P., Fluke C. J., 2000, MNRAS, 319, 267
 Bartelmann M., Schneider P., 2001, Physics Reports, 340, 291
 Bernardeau F., Van Waerbeke L., Mellier Y., A&A, 1997, 322, 1
 Blandford R. D., Saust A. B., Brainerd T. G., Villumsen J. V., 1991, MNRAS, 251, 600
 Brown M. L., Taylor A. N., Hambly N. C., Dye S., 2000, astro-ph/0009499
 Couchman H. M. P., Barber A. J., Thomas P. A., 1999, MNRAS, 308, 180
 Couchman H. M. P., Thomas, P. A., Pearce F. R., 1995, ApJ, 452, 797
 Hamana T., Colombi S., Mellier Y., 2000, Proc. of XXth Morion Astrophysics Meeting, ed., Kneib J.-P., Mellier Y., Mon M., Van Thanh J. T.
 Hamilton A. J. S., Matthews A., Kumar P., Lu E., 1991, ApJ, 274, L1
 Heavens A., Refregier A., Heymans C., 2000, MNRAS, 319, 649
 Jain B., Seljak U., ApJ, 1997, 484, 560
 Jain B., Seljak U., White S., 2000, ApJ, 530, 547
 Kaiser N., 1998, ApJ, 498, 26
 Kaiser N., Wilson G., Luppino G. A., 2000, astro-ph/0003338
 Maoli R., Van Waerbeke L., Mellier Y., Schneider P., Jain B., Bernardeau F., Erben T., Fort B., 2001, A&A, 368, 766
 Mellier Y., Van Waerbeke L., Maoli R., Schneider P., Jain B., Bernardeau F., Erben T., Fort B., 2001, astro-ph/0101130
 Peacock J. A., Dodds S. J., 1996, MNRAS, 280, L19
 Peacock J. A., Smith R. E., 2000, MNRAS, 318, 1144
 Premadi P., Martel H., Matzner R., Futumase T., 2001, astro-ph/0101359
 Rhodes J., Refregier A., Groth E. J., 2001, ApJ, 552, 85
 Schneider P., Ehlers J., Falco E. E., 1992, 'Gravitational Lenses,' Springer-Verlag, ISBN 0-387-97070-3
 Scoccimarro R., Couchman H. M. P., 2001, MNRAS, 325, 1312
 Seljak U., 2000, MNRAS, 318, 203
 Van Waerbeke L., Mellier Y., Erben T., Cuillandre J. C., Bernardeau F., Maoli R., Bertin E., McCracken H. J., Le Fèvre O., Fort B., Dantel-Fort M., Jain B., Schneider P., 2000a, A&A, 358, 30
 Van Waerbeke L., Mellier Y., Erben T., Cuillandre J. C., Bernardeau F., Maoli R., Bertin E., McCracken H. J., Le Fèvre O., Fort B., Dantel-Fort M., Jain B., Schneider P., 2000b, A&A, 358, 30
 Van Waerbeke L., Hamana T., Scoccimarro R., Colombi S., Bernardeau F., 2001a, MNRAS, 322, 918
 Van Waerbeke L., Mellier Y., Radovich M., Bertin E., Dantel-Fort M., McCracken H. J., Le Fèvre O., Foucaud S., Cuillandre J. C., Erben T., Jain B., Schneider P., Bernardeau F., Fort B., 2001b, A&A, 374, 757
 Wittman D. M., Tyson J. A., Kirkman D., Dell'Antonio I., Bernstein G., 2000, Nature, 405, 143